The Journal of Chemical Physics

The susceptibility of α-helical secondary structure to steric strain: Coarse-grained simulation of dendronized polypeptides

Cite as: J. Chem. Phys. **133**, 145102 (2010); https://doi.org/10.1063/1.3498780
Submitted: 06 April 2010 . Accepted: 17 September 2010 . Published Online: 11 October 2010

William Browne, and Phillip L. Geissler

The susceptibility of α-helical secondary structure to steric strain: Coarse-grained simulation of dendronized polypeptides

William Browne and Phillip L. Geissler[a)]
Department of Chemistry, University of California at Berkeley, Berkeley, California 94720, USA

(Received 6 April 2010; accepted 17 September 2010; published online 11 October 2010)

The propensity of a peptide chain for adopting helical secondary structure can be modulated not only through the solvation properties of its side chains but also through their size and shape. Here we examine a coarse-grained model for dendronized polypeptides that focuses on the susceptibility of α-helical structure to the steric strain exerted by hydrophilic pendant groups. Undecorated molecules exhibit a pronounced transition from random coil to helix upon cooling [J. P. Kemp and J. Z. Y. Chen, Biomacromolecules **2**, 389 (2001)]. As gauged by specific heat and by order parameters characterizing helicity at several length scales, this transition is quite robust to the introduction of first- and second-generation dendron side chains. More highly branched side chains, however, reduce the entropy of compact states so severely that helical ordering is undetectable over the entire temperature range accessible to our importance sampling methods. Consistent with experimental observations for side chains comparable to those of our model in volume-excluding size and shape, we find the backbone of these third-generation molecules to assume a distended rodlike state that is both stiff and achiral. © *2010 American Institute of Physics*.
[doi:10.1063/1.3498780]

I. INTRODUCTION

A nuanced interplay of entropic and enthalpic factors stabilizes α-helices, the most abundant secondary structure in proteins.[1] Free energy contributions that stabilize this structure are either extrinsic, originating from the medium in which the structure exists, or intrinsic, deriving from intramolecular properties of the peptide segment. Extrinsically, the stability of α-helices in proteins is often aided by helix capping where the termini of a helical segment has dangling hydrogen bond acceptors or donors that engage with partners elsewhere in its protein.[2] In addition, weak solvent polarity, as for hexane or octanol, and local environments in which the backbone is protected from aqueous solvent are known to stabilize helices. Their favorability in nonpolar environments is a result of the stability of the hydrogen bonding network along the helical core, which water can compromise by acting as a hydrogen bonding partner to a backbone amide hydrogen or carbonyl oxygen. Thus, in water, the helix needs shielding from solvent, rendering intrinsic contributions from intrasegment side chains greatly important for stabilizing helical structure. One example of this phenomenon is the protection afforded by clustering of hydrophobic side chains. This sequestration from solvent within a compact greasy aggregate makes peptides enriched in amino acids like alanine good helix formers. Another important intrinsic contribution to helix free energy comes from the entropy of side chains. Side chains on the outside of the helical barrel are significantly constrained in their movement, effecting an unfavorable loss of entropy.[3] Adjusting the interactions between the side chains by altering temperature, ionic strength, *p*H, and primary sequence can reinforce or alleviate these constraints. For example, lysine homopolymer α-helices are stable at *p*Hs above the pKa at which the terminal amino group becomes positively charged. Exploiting these physical mechanisms, several research groups have successfully manipulated the thermodynamic stability of this secondary structure using an array of extrinsic and intrinsic control variables.[4–8]

Perhaps the most fundamental of the variables that control peptide secondary structure is primary structure. The amino acids that comprise the units of primary structure present side chains that have distinct hydrophobicity, charge, shape, and propensity for hydrogen bonds. Conceivably, all of these properties can participate in the creation and stabilization of secondary structure and often must be considered collectively to explain why a backbone adopts a specific conformation. For example, peptide chains comprised of β carbon substituted amino acids such as valine do not adopt helical structures, while helix stability is conferred by leucine, an amino acid of similar size and composition but branched instead at the γ carbon. This phenomenon, for hydrophobic residues at least, has been shown by Monte Carlo simulations to arise from entropy losses due to restrictions on side chain fluctuations.[3,9] It invites the question of whether a similar phenomenon exists for hydrophilic residues, which present a more diverse range of enthapic influences on helix stability. For example, hydrophilic side chains can form hydrogen bonds both with other side chains and with backbone moities, possibly bridging long segments of the chain.

The α-helical dendronized polymers such as those synthesized by Lee *et al.*[10] are an excellent model system for assessing the influence pendant hydrophilic groups exert on this secondary structure. Dendronized polymers consist of oligomeric units whose side chains have steric bulk that in-

[a)]Electronic mail: geissler@cchem.berkeley.edu.

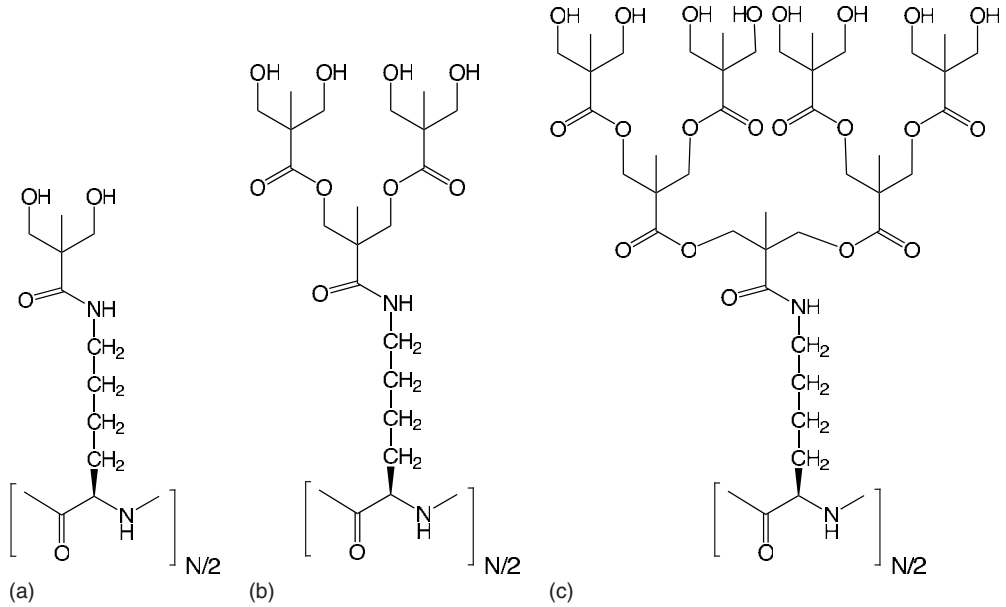

FIG. 1. Chemical structures of first (a), second (b), and third (c) generation polyester dendrons attached to a peptide backbone as synthesized by Lee *et al.* (Ref. 10). Each consists of a peptide backbone, a lysine connector chain, and an attached dendron.

creases exponentially with generation number, N_g (see Fig. 1). Interactions that might stabilize an α-helical dendronized polymer include backbone-backbone hydrogen bonding and the aggregation of hydrophobic connecting units that link branched side chains to the peptide backbone. Opposing these forces, decreased rotameric entropy and backbone-side chain hydrogen bonding should exert a net destabilizing effect on backbone structure.[11] So, given an α-helix-forming homopeptide with hydrophilically terminated side chains like this particular polymer, should increasing the size of the side chains destroy helicity in analogy to the way β-branched peptides lose theirs? This question is especially pertinent to assessing the dominance of entropic contributions over enthalpic effects related to the hydrophilicity of the dendritic side chains. We find that a reduction of side chain entropy in compact states can alone drive the loss of helicity for a polymer with hydrophilic side chains. Because we are interested in the properties of a single electroneutral peptide, we focus on intrinsic factors such as rotameric entropy, backbone-side chain hydrogen bonding, backbone-backbone hydrogen bonding, and hydrophobic side chain interactions, ignoring Coulombic and protein-dependent factors such as helix capping or the segregation of entire segments of peptide into nonaqueous environments, such as a cell membrane or a hydrophobic portion of a protein.

The computational work described in this paper concerns the α-helical dendronized polymers synthesized by Lee *et al.*, which exhibit a sharp change in their secondary-structural character, measured by circular dichroism (CD), as N_g increases. Our coarse-grained molecular approach to exploring the etiology of this transition distinguishes between potential mechanisms by selectively including or omitting particular aspects of peptide interactions. Due to the very large number of atoms per helical loop and the large fluctuations characteristic of a helix-coil phase transition, a method that eschews atomistic detail is in fact necessary to gather representative equilibrium statistics within a reasonable amount of time. As described in Sec. II, the minimal model we study is based on a helix-forming, freely rotating chain that is known, in the absence of side chains, to capture important thermodynamic signatures of helical ordering in peptides.[12] In Secs. III and IV, we briefly discuss the techniques we employ to model this dendronized polymer. Section V describes quantities and methods we use to characterize energy fluctuations and helical ordering along the polymer backbone.

Simulation results are presented in Sec. VI. Our primary findings concern robustness of the helical ordering transition to the introduction of sterically restrictive side chains. For small enough N_g, our model exhibits only mild changes in conformational statistics relative to a molecule without side chains. When the generation number is increased from $N_g=2$ to $N_g=3$, the steric bulk of the side chains alone are sufficient to induce a sharp loss of helical ordering, which is in agreement with CD spectra taken by Lee *et al.* In other words, we find that a simple model, describing only an inherent propensity for helical ordering and volume exclusion among bulky side chains and backbone, can capture observed changes in secondary structure of a dendronized polymer. Interestingly, the model third-generation polymer maintains a helical ground state consistent with steric constraints. Thus, its lack of helicity at ambient conditions results from dendron fluctuations becoming so strongly curtailed in the ordered state that the backbone's decreased energy cannot compensate for the side chains' lost entropy. In Sec. VII, we conclude.

II. MODEL

We have adapted a coarse-grained picture of helix-forming peptide backbones[13,14] in order to explore the influ-

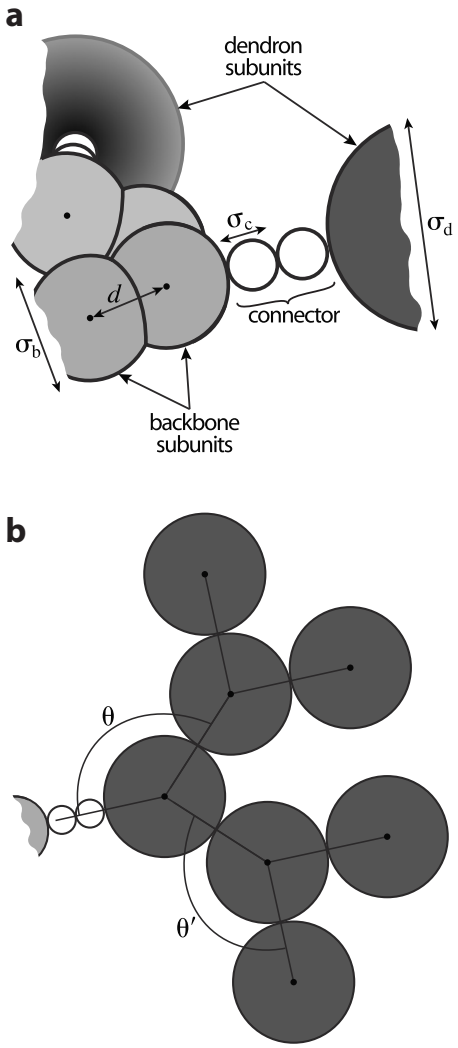

FIG. 2. Geometry of our model for dendronized polypeptides. Panel (a) shows a cutout segment of the backbone with connector units and dendron subunits attached. Panel (b) shows a single connector and third-generation dendron side chain. The relative dimensions of these various moieties are correct within both panels.

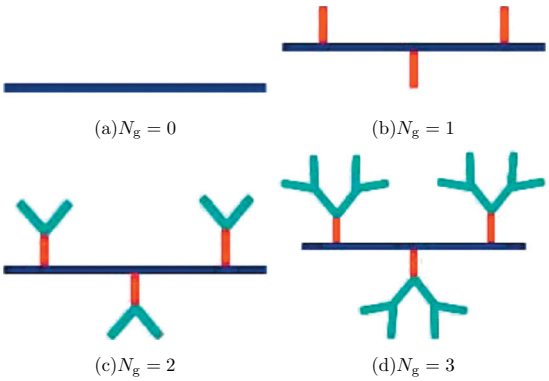

FIG. 3. Schematic representation of molecules with successively larger values N_g. The blue line represents the backbone. The red lines represent the connector units and their attached first-generation dendron subunits. Turquoise branches represent additional dendron subunits. Side chain environments are much more crowded than depicted here.

ence of dendritic side chains on conformational fluctuations. The basic structural elements and geometry of our model are sketched in Figs. 2 and 3.

The potential energy and constraints associated with backbone arrangements are taken directly from Ref. 14. Each residue's main chain atoms are represented by a pair of identical backbone subunits. The separation between each pair of consecutive subunits is fixed at a distance d, which we adopt as a reference length scale. The vector pointing from the center of subunit i to that of the next subunit along the chain, $i+1$, can thus be written as $d\hat{\mathbf{t}}_i$, where $\hat{\mathbf{t}}_i$ is a unit bond vector. The angle between consecutive bond vectors is fixed at $\pi/3$, i.e., $\hat{\mathbf{t}}_i \cdot \hat{\mathbf{t}}_{i+1} = 1/2$. Absent further constraints of excluded volume and interactions favoring helical order, the backbone would thus comprise a freely rotating chain of $N-1$ links.

Helicity is encouraged through a potential energy

$$U = \epsilon \sum_{i=1}^{N-1} \sum_{j=i+2}^{N-1} u(\hat{\mathbf{b}}_i, \hat{\mathbf{b}}_j, \mathbf{r}_{ij})$$

that rewards winding of the backbone and enforces steric constraints that disallow overlap of aligned chain segments. Here, ϵ is a positive constant parameter that represents the strength of the potential. In practice, this parameter should be adjusted so that corresponding thermodynamic transitions, e.g., the coil to helix transition, match those of the actual system under consideration. In detail,

$$u(\hat{\mathbf{b}}_i, \hat{\mathbf{b}}_j, \mathbf{r}_{ij}) = \begin{cases} 0 & r_{ij} > r_{\text{cut}} \\ -(\hat{\mathbf{r}}_{ij} \cdot \hat{\mathbf{b}}_i)^6 - (\hat{\mathbf{r}}_{ij} \cdot \hat{\mathbf{b}}_j)^6, & d < r_{ij} < r_{\text{cut}} \\ \infty, & r_{ij} < d, \end{cases}$$

where r_{ij} is the distance between subunits i and j, $\hat{\mathbf{r}}_{ij}$ is the unit orientation of the separation vector between subunits i and j, and $\hat{\mathbf{b}}_i = \hat{\mathbf{t}}_{i+1} \times \hat{\mathbf{t}}_i / |\hat{\mathbf{t}}_{i+1} \times \hat{\mathbf{t}}_i|$ is the chain's unit binormal vector at subunit i.

Backbone subunits have a volume-excluding diameter $\sigma_b = 1.5d$. (Consecutive subunits, whose separation distance is fixed at $d < \sigma_b$, are exempt from constraints of volume exclusion.) The cutoff at $r_{\text{cut}} = \sqrt{45/2}d$ mimics the short range of hydrogen bonding interactions responsible for attractions within the peptide's main chain. The ground states of this backbone potential are left- and right-handed helices with six subunits (i.e., three amino acid residues) per complete turn. Canonical right-handed α-helix secondary structures wind somewhat more gradually, with approximately 3.6 residues per turn. Further details about the backbone model can be found in Ref. 14.

Helix formation in aqueous solvent occurs in part because water is shielded from the helical core. Thus, for a peptide without side chains (e.g., poly-G), helical configuration is unstable for real polypeptides. As such, we view the energetics and the structures this backbone model produces as implicitly describing the role of small hydrophobic side chains in shielding the backbone from solvent. For a full discussion of the backbone model as well as a more complete discussion of its thermodynamics, see Ref. 14.

Atomistically detailed models using the CHARMM force field for side chain-bearing peptides have shown that

helical order sets in sharply when T is lowered concomitant with large energy fluctuations. The backbone model shows this behavior, establishing a firm correspondence with highly detailed models of several homopolypeptides with side chains. In synthetic dendritic polymers, the shielding role of these natural side chains can be played by the connecting groups that link side chain to backbone, which are hydrophobic in character.

Attached to every second subunit ($i=1,3,5,\ldots$) is a dendron side chain comprising a two-bead connector and one or more dendron subunits (see Fig. 2). Connector beads are assigned a volume-excluding diameter $\sigma_c=0.6d$, and dendron subunits a diameter $\sigma_d=2.6d$, roughly capturing the sizes of respective chemical moities in the molecules synthesized by Lee *et al.*[10] The first connector bead lies in contact with the backbone subunit; the second connector bead contacts the first; and the first dendron subunit contacts the second connector bead. As drawn in Fig. 2, the centers of these three spheres, as well as the backbone subunit, all lie on a straight line, whose orientation is biased only by steric interactions with other parts of the molecule.

For second- and third-generation polymers, additional dendron subunits branch off from the first. For $N_g=2$, two subunits are connected to the first. The angle θ defined by a second-generation dendron subunit, the first-generation subunit, and the backbone subunit is maintained very close to $\theta_0=133.7°$ by a potential energy $\epsilon'(\cos\theta-\cos\theta_0)^2$, with $\epsilon'/k_BT=2555$. The distance $r_{(1,2)}$ between first- and second-generation subunits is also tightly regulated, executing only small fluctuations about the contact length σ_d due to a potential $k(r_{(1,2)}-1.1d)^2$, with $kd^2/k_BT=1$.

In a similar manner, for $N_g=3$, two third-generation dendron subunits are connected to each second-generation subunit. Here, the angle θ' defined by a triad of first-, second-, and third-generation dendron subunits is held very near θ_0 by a potential harmonic in $\cos\theta'$ with force constant ϵ', and the distance $r_{(2,3)}$ between connected second- and third-generation subunits is strongly biased by the energy $k(r_{(2,3)}-1.1d)^2$. The purpose of allowing these dendron parameters (θ, $r_{(1,2)}$, θ', and $r_{(2,3)}$) to vary at all is to facilitate construction of sterically permissible starting configurations for sampling of densely packed states.

Like nominally hydrophilic amino acids, dendron side chains have hydrophobic portions. Common to all generations is the hydrophilic terminus of the side chain. Thus, in our model, the end of the side chains' exposure to solvent does not incur thermodynamic cost. We do not attempt to explicitly represent hydrogen bonds they might form with each other or with the backbone. Side chain-backbone hydrogen bonding is unlikely in any case because of the entropic penalty a chain would have to pay to satisfy a configuration that would accommodate side chain terminus-backbone contact.

III. SIMULATIONS

We used Monte Carlo simulations to determine probability distributions and ensemble averages for model dendritic polymers with $N_g=0$ (lacking dendron side chains), $N_g=1$ (one dendron subunit per monomer), $N_g=2$ (three dendron subunits per monomer), and $N_g=3$ (seven dendron subunits per monomer). Trial moves include (1) the displacement of a backbone subunit and its corresponding side chain by crankshaft rotation on $[0,2\pi)$ about the axis defined by the two backbone subunits that proceed toward the center of the chain; (2) the displacement of a dendron side chain by a free rotation about Euler angles (θ,ϕ,ψ) on $([0,2\pi),[0,\pi),[0,2\pi))$ centered at the parent subunit, keeping the internal structure of the side chain fixed; and (3) the movement of a second- or third-generation dendron subunit to a random point uniformly distributed within a cube of side length d centered at its current position. The last of these moves is effective only during early stages of a simulation, while dendron side chains' internal structures relax from a highly regular initial configuration. Following this equilibration period, such displacements are nearly always rejected.

In straightforward simulations, all trial moves are accepted or rejected according to the Metropolis criterion. This sampling approach is only practical, however, at temperatures sufficiently high that the polymer backbone does not adopt a compact conformation. For temperatures lower than $\approx 2\epsilon/k_B$, typical configurations are very densely packed, and average acceptance probabilities for trial moves of appreciable magnitude drop sharply. In this regime, which encompasses the transitions of interest, advanced sampling techniques are necessary to properly survey the range of thermodynamically relevant structures. For this purpose, we have used and extended Wang and Landau's method for sampling microstate distributions that span fluctuations typical of a broad range of temperatures.

IV. WANG–LANDAU SAMPLING

For molecules with $N_g=0$, $N_g=1$, and $N_g=2$, we used Wang–Landau sampling techniques[15] to adaptively achieve a uniform sampling of energies, i.e., to determine the density of states $D(E)$. Third-generation polymers, in which the packing of side chains for compact backbone conformations is extremely tight, present exceptional sampling difficulties that are not fully abated by these standard methods. To address this problem, we introduced a bias on a second parameter ξ_{pack} that characterizes side chain packing,

$$\xi_{pack}=\frac{1}{M-1}\sum_{i=1}^{M-1}|\mathbf{r}_{i+1}-\mathbf{r}_i|,$$

where $\mathbf{r}_i$ is the position of the first-generation dendron subunit of the ith dendron and $M=N/2$. This additional bias facilitates transitions among compact states by making intermediate extended states more accessible. In this case, an extended Wang–Landau scheme[16] was used to construct a weight function of both U and ξ_{pack} that yields a uniform two-dimensional histogram $H(U,\xi_{pack})$.

Sampling the density of states for third-generation polymers was further aided by apportioning sampling among several windows with overlapping energy ranges. We established these ranges in a systematic way that gauges typical losses in sampling efficiency as energy decreases. In detail, we first initiate a Wang–Landau sampling procedure that

would ultimately generate a histogram uniform in U and ξ_{pack}. A reasonable degree of uniformity is almost invariably achieved at high energies before low-energy states are extensively sampled. Exploiting this tendency, we identify when approximate uniformity has been achieved over an appreciable range of energy, i.e., when negative deviations of $H(U,\xi_{\text{pack}})$ from its average value are at most 20% for all accessible values of ξ_{pack} and for energy values in the interval $U_{\text{min}}^{(0)} < U < U_{\text{max}}^{(0)}$. The value $U_{\text{max}}^{(0)}$ is the mean energy at infinite temperature. The coordinate ξ_{pack} is bounded by empirical values that avoid extremes. Should the width of the interval $U_{\text{max}}^{(0)} - U_{\text{min}}^{(0)}$ exceed a threshold value of 2ϵ, we cease sampling (otherwise continuing until the threshold criterion is met). The lower limit $U_{\text{min}}^{(0)}$ is then used to define a new sampling window, in which energy is constrained to values below $U_{\text{max}}^{(1)} = U_{\text{min}}^{(0)} + \mathcal{W}$. The small overlap $\mathcal{W} = \epsilon$, provides a region to compute an optimal overlap of adjoining histograms. We simply match values at $U_{\text{max}}^{(n)}$ and $U_{\text{min}}^{(n-1)}$, though more sophisticated algorithms to compute optimal overlap of the n^{th} and $(n+1)^{\text{th}}$ segments of $H(U,\xi_{\text{pack}})$ in the region $[U_{\text{min}}^{(n)}, U_{\text{max}}^{(n+1)}]$ are possible. This protocol is repeated in the new window (sampling until uniformity is achieved in an interval $U_{\text{min}}^{(n-1)} < U < U_{\text{max}}^{(1)}$ of width exceeding 2ϵ), setting a bound for sampling in a third window, $U_{\text{max}}^{(2)} = U_{\text{min}}^{(1)} + \mathcal{W}$, and so on. In order to avoid very narrow windows, we require that $U_{\text{max}}^{(n)}$ lies at least 2ϵ above $U_{\text{min}}^{(n-1)}$ for all n.

When this process reaches the bottom of the intended energy range, we join the series of histograms and assemble the set of weight functions into a two-dimensional density of states (depending on both U and ξ_{pack}). We then repeat the entire process with a smaller value of the Wang–Landau reweighting factor with the prescription $f_{\text{j}} = \text{e}^{1/j}$, where j denotes the iteration of the process described above. Finally, we determine $D(E)$ by integrating numerically over ξ_{pack}.

V. CONFORMATIONAL STATISTICS

We characterize the onset of helical ordering with decreasing temperature following Ref. 14 through a set of functions $H^{(1)}$, $H^{(2)}$, and $H^{(3)}$ that quantify the alignment of backbone binormal vectors over short, intermediate, and long ranges, respectively. Correlations between consecutive binormals, which give a sense for the degree of local coiling, determine

$$H^{(1)} = \sum_{i=2}^{N-1} \hat{\mathbf{b}}_{i-1} \cdot \hat{\mathbf{b}}_i. \tag{1}$$

While $H^{(1)}$ does not provide a discriminating signal for the cooperative development of helical order accompanying a phase transition, its focus on local structure resonates with traditional views of α-helix stability due to intrabackbone hydrogen bonding. The persistence of coiling in a certain direction over a larger stretch of the chain is obtained by comparing all binormal vectors with that at the chain's midpoint,

$$H^{(2)} = \sum_{i=1}^{N-1} \hat{\mathbf{b}}_i \cdot \hat{\mathbf{b}}_{\text{mid}}, \tag{2}$$

where $\mathbf{b}_{\text{mid}} = \mathbf{b}_{\text{floor(N/2)}}$. The floor function rounds down to the nearest integer. Finally, helicity of the chain as a whole is captured by the average magnitude of net alignment,

$$H^{(3)} = \left| \sum_{i=1}^{N} \hat{\mathbf{b}}_i \right|. \tag{3}$$

The spatial extent of the polymer is measured by its radius of gyration,

$$R_{\text{g}} = N^{-1/2} \sqrt{\sum_{i=1}^{N} |\mathbf{q}_i - \mathbf{q}_{\text{cm}}|^2}. \tag{4}$$

where $\mathbf{q}_i$ is the position of the ith backbone subunit and $\mathbf{q}_{\text{cm}}$ is the center of mass of the backbone. For very long chains, $\langle R_{\text{g}}^2 \rangle$ should scale as N^2 for the helical state, as $N^{2/3}$ for a compact globular state, and as N for a random coil. In the limit $N \to \infty$, rigid helical configurations are therefore considered to be largest by this measure, followed by random coil and then compact globule.

VI. RESULTS AND DISCUSSION

The thermodynamic properties of the backbone model we use were computed in the absence of side chains by Kemp and Chen. A pronounced maximum in the specific heat C_v at $T = 1.2\epsilon/k_{\text{B}}$ signals a transition between states distinguished both by the chain's overall size and by the extent of helical alignment. The growth of this peak with chain length indicates a corresponding cooperativity over length scales exceeding the size of molecules they studied ($N < 40$). Comparing the degree of this cooperativity to that of helix formation in real peptides is made difficult by a lack of extensive finite size scaling data for C_v from experiment. Parameters assessing cooperativity through the correspondence of calorimetric energy differences and those implied by the temperature dependence of helical order parameters are not well-suited to Kemp and Chen's model due to the juxtaposition of collapse and helical ordering transitions. As a rough comparison, we have calculated the scaling of peak heat capacity with chain length for a model formulated and parameterized to capture the thermodynamics of helix formation in Baldwin's peptides.[17] Results are very similar to those for the backbone model we use here. For $N_g > 0$, the peak in C_v grows more strongly with N, indicating a higher degree of cooperativity in the presence of side chains.

More subtle features of C_v at low temperature ($T \approx 0.3\epsilon/k_{\text{B}}$) mark the compaction of the ordered chain into a tightly bundled, large-aspect ratio helix. Reference 14 emphasized as well a crossover between random coil-like structures at high temperature and globular conformations, rich in intrachain contacts but lacking long-range helical order, at intermediate T. This latter change, however, is accompanied neither by sharp changes in order parameters such as $\langle R_g^2 \rangle$ and $\langle H^{(i)} \rangle$ nor by diverging susceptibilities. We therefore focus on the influence of dendron side chains on the pro-

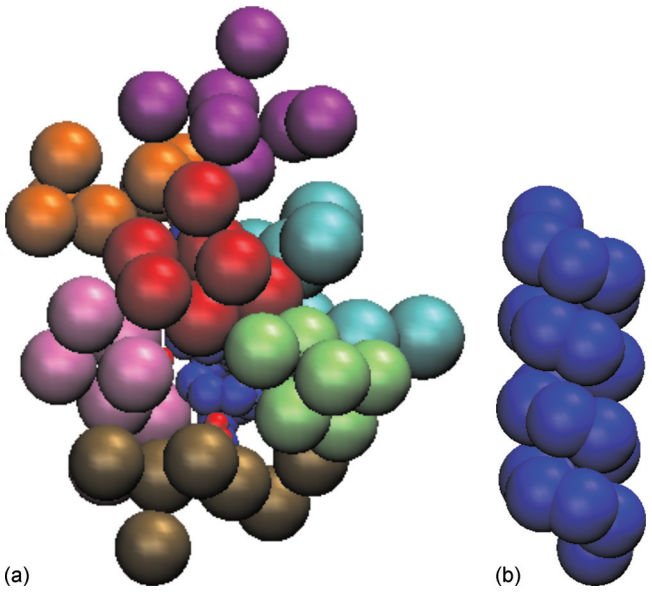

FIG. 4. Example of a sterically permissible configuration of a third-generation polymer with strong helical order. Side chains are shown in (a), each colored differently to highlight dendron subunit connectivity. The backbone conformation is shown in (b) without side chains to reveal helicity. This configuration, generated in the course of Wang–Landau sampling, represents an extreme minority at all temperatures for which we report quantitative results.

nounced ordering transition at $T=1.2\epsilon/k_B$ and on structural and thermodynamic properties of the helical state.

The introduction of first- and second-generation dendron side chains effects remarkably little change in the overall thermodynamics of helical ordering. As shown in Fig. 5, C_v peaks more sharply but at nearly the same temperature as in the absence of side chains. A careful inspection of structural order parameters, plotted as functions of T in Fig. 7, suggests, however, that underlying this robustness is a balance between competing influences.

Backbone structures of our model polypeptides are sensitive to the presence of side chains in two related ways. First, steric constraints imposed by pendant, volume-excluding groups disallow some backbone conformations entirely. One might expect low-energy helical structures, which

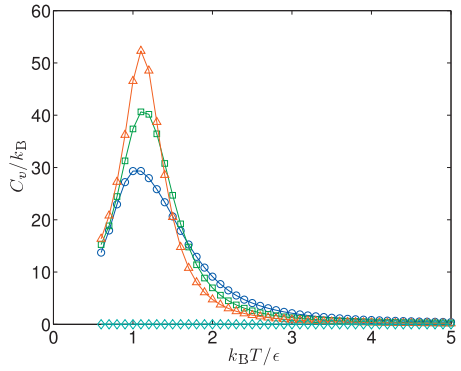

FIG. 5. Heat capacity as a function of temperature for chains of length $N=22$ with generation numbers $N_g=0$ (○), $N_g=1$ (□), $N_g=2$ (△), and $N_g=3$ (◇). The peak in the specific heat indicates the temperature coordinate of the helix-coil transition. Each curve was obtained by numerical differentiation of the average energy, determined by integration of the density states determined by Wang–Landau sampling.

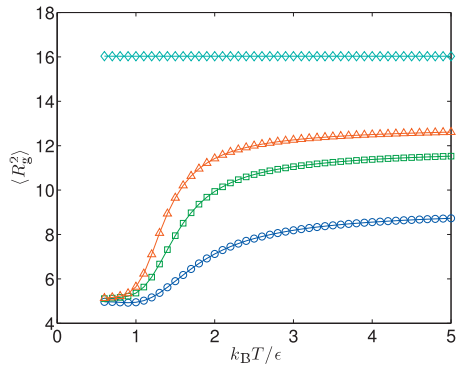

FIG. 6. The squared radius of gyration as a function of temperature for a polymer of length $N=22$. Results are shown for $N_g=0$ (○), $N_g=1$ (□), $N_g=2$ (△), and $N_g=3$ (◇). Curves were obtained by first calculating $\langle R_g^2 \rangle_E$, the average value of R_g^2 within a small interval of energy centered on E, in the course of Wang–Landau sampling. Thermal averages were then constructed by summing $\langle R_g \rangle_E D(E) e^{-E/k_BT}/Q$ over the range of sampled energies, where $D(E)$ is the density of states and $Q=\Sigma_E D(E) e^{-E/k_BT}$ is the canonical partition function at temperature T.

crowd the immediate environment of every backbone subunit, to suffer most strongly from this imposition. However, our results argue against a uniformly increasing severity of backbone entropy loss with increasing helicity. Were the simple expectation correct, the onset of helical order would shift to lower temperature: the inability to access low-energy conformations would both lessen the energetic benefit of adopting helical structures and exacerbate the corresponding entropic penalty. On the contrary, for $N_g=1$ and $N_g=2$, the peak in C_v resides at a slightly *higher* temperature than for $N_g=0$. Furthermore, all three helical order parameters indicate that the helical states of the low-generation dendronized molecules are in fact more strongly ordered than their dendron-less counterparts.

The second way in which side chains can bias backbone structure, which explains the upward shift in ordering temperature for $N_g=1$ and $N_g=2$, is more subtly statistical in nature. The backbone conformations that permit greatest freedom in dendron subunit placement have the highest statistical weights at equilibrium. (The prohibition against conformations that are inconsistent with any sterically admissible dendron placement is nothing more than an extreme instance of this effect.) In rough terms, this bias suppresses doubling back of the chain contour into regions it has already explored. For the high-temperature coil state, which is already sparse in long-range contacts, the primary consequence should be an effective local stiffening of the backbone. This statistical, rather than simply energetic, increase in rigidity is apparent in the growth of $\langle R_g^2 \rangle$ with dendron generation number, as shown in Fig. 6. Side chain induced swelling, and in particular steric enhancement of persistence length, has been reported and discussed for similarly branched chain molecules.[18]

Because conformational distributions of the coil state are significantly more constrained at $N_g=1$ and $N_g=2$, its entropy is substantially reduced from that of the self-avoiding random flight at $N_g=0$. This entropic loss is accompanied by increases in average energy, as reflected in Fig. 7(a) by deterioration of helical order. These changes in the coil's free

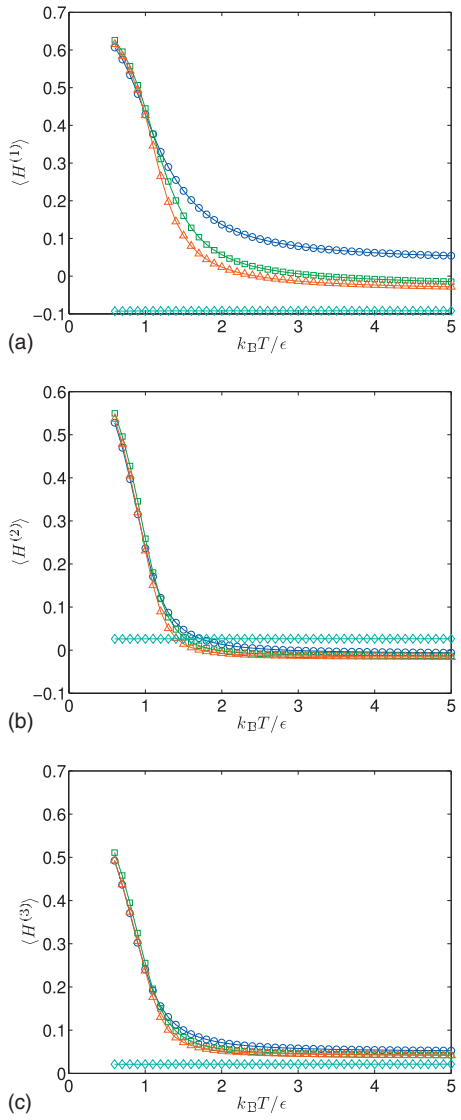

FIG. 7. Helical order parameters $H^{(1)}$,$H^{(2)}$, and $H^{(3)}$ as functions of temperature for a polymer with $N=22$. Results are shown for $N_g=0$ (○), $N_g=1$ (□), $N_g=2$ (△), and $N_g=3$ (◇). As for Fig. 6, these thermal averages were computed as Boltzmann-weighted sums over microcanonical averages of each structural order parameter.

energy nearly balance those of compact states, resulting in a helix-to-coil transition temperature that is only slightly modified. That the shift in transition temperature is positive indicates that the dendron-induced restrictions on coil fluctuations are thermodynamically more severe (though marginally so). The effect of side chains shifting ordering transitions to higher temperatures has been noted for similar molecules in Ref. 19.

Dendron-induced swelling is also evident in the helical state of first- and second-generation molecules. As measured by increases in $\langle R_g^2 \rangle$ over the $N_g=0$ case, this effect is much weaker than for the high-temperature coil. The distended helix furthermore does not suffer loss of binormal vector alignment and lies lower in energy on average than an undecorated backbone at the same temperature. This somewhat counterintuitive behavior suggests an analogy with the situation underlying thermodynamic stability of hard sphere crystalline solids at high pressure: Among (backbone) configurations with high local density, ordered arrangements provide the most flexibility for accommodating fluctuations in remaining degrees of freedom. For a collection of hard spheres, these remaining fluctuations comprise small-amplitude, short-wavelength vibrations about inherent structures. For our model of dendronized polypeptides, they instead involve packing of branched side chains in the space that is not excluded by the backbone. Backbone configurations with modest helical order evidently constrain side chain motions more severely than do more ideal helix structures. This conclusion is essentially implicit in the results in Ref. 20, which show that volume-excluding side chains can induce helical order even for a model backbone with no inherent energetic preference for helicity.

Though operating through the same mechanisms, the influence of dendron side chains becomes much more dramatic at third generation. Just as the constraints of secondary branching hinder effective Monte Carlo sampling, so do they render all but the most extended backbone conformations nearly irrelevant in statistical terms. All of the thermodynamic and structural parameters we have discussed are essentially athermal for $N_g=3$ over the entire range in which we could obtain reliable statistics. The radius of gyration ($\sqrt{\langle R_g^2 \rangle} \approx 4$) is close to its maximum allowed value ($R_g^{(\max)}=5.5$), corresponding to near maximal extension with the rigid bond angles we have imposed), and the average energy from backbone stacking interactions is negligible (as are fluctuations in this energy, hence $C_v \approx 0$). The computed value of $H^{(1)}$ even differs in sign from those of $N_g<3$ molecules, highlighting antialignment of adjacent binormal vectors as a means of resolving severe local strain.

From these facts, it is tempting to infer that third-generation dendron side chains are simply too large to be accommodated in helical conformations. While this notion may as well be correct for practical purposes, it is nonetheless interesting that sterically permissible ordered configurations do exist at $N_g=3$. One example, identified in the course of Wang–Landau sampling at low energy, is shown in Fig. 4. At some very low but finite temperature, the helical state must therefore become thermodynamically stable. Profound sampling difficulties prevent us from making a useful estimate of this temperature. However, the single example we have presented establishes that even in this extreme case of side chain crowding, operative thermodynamic biases are of the more subtle statistical variety. In other words, finite but large changes in entropy, rather than geometric impossibility, are responsible for the loss of helical order in our simulation results.

Experimental data also show that helicity is lost at $N_g=3$. This invites speculation that as in the case of other dendronized polymers, the steric repulsions described by our model are responsible for compromising helical order. The more subtle thermodynamic consequences of these repulsions at lower generation numbers are also echoed by counterintuitive trends observed in experiments. For example, circular dichroism measurements show a more intense α-helical signature for second-generation dendrons than for first-generation dendrons. Previous simulations have suggested

that dendrons aid the formation of helices (Ref. 21). Our simulations confirm this notion explicitly for second-generation dedrimers.

VII. CONCLUSIONS

We have presented a scenario for loss of secondary structure in alpha-helix-forming polymer backbones due to bulky hydrophilic side chains that is dominated by entropic consequences of steric constraints. In particular, nontrivial behavior in accord with experimental observations emerges from a model lacking any description of hydrogen bonding or solvation. While these enthalpic contributions involve potent forces, we argue that the solventlike character of dendron side chains provides such diverse possibilities for realizing strongly favorable interactions that the energetic bias on backbone structure is weak. As a result, side chain volume exclusion dominates in shaping thermal ensembles of chain conformations. Points of agreement between our calculations and experimental measurements do not rule out involvement of solvent in the helix-breaking transition, but they do support the view that entropy changes are primarily responsible for disrupting helical order.

In our simulations, the instability of ordered backbone conformations in the presence of highly branched side chains is more subtle than might be anticipated from simple notions of molecular shape. At $N_g=1$ and $N_g=2$, the principal effect of volume exclusion is an effective backbone stiffening whose thermodynamic consequences are most strongly felt in the disordered coil-like state. At $N_g=3$, ordering is possible in principle, i.e., we have identified sterically permissible configurations that exhibit extensive helicity but impose strict limitations on dendron fluctuations that are entropically prohibitive except at very low temperatures. This intriguing prediction is not straightforward to assess in experiments. As in many coarse-grained biomolecular models, the scale ϵ of interactions can be considered a constant parameter for realistic systems only over the narrow range of temperature in which solvent properties do not change appreciably.

The approach we have taken to explore the susceptibility of secondary structure to steric strain could be applied to examine other kinds of perturbations and could be extended to study larger systems comprising domains with greater structural variability. For example, one might consider a protein with α-helical and random coil subdomains, applying our treatment of side chain-bearing helices along with simple descriptions of the random coil domains. Our model could also be amended with an explicit treatment of hydrogen bonding and the preference of hydrophilic moieties for polar environments, as a direct test of the principal assumptions we have made.

[1] W. Kabsh and C. Sander, Biopolymers **22**, 2577 (1983).
[2] G. D. Rose, Nat. Chem. Biol. **2**, 123 (2006).
[3] B. W. Chellgren and T. P. Creamer, Proteins: Struct., Funct., Bioinf. **62**, 411 (2006).
[4] D. Eisenberg, W. Wilcox, S. M. Eshita, P. M. Pryciak, S. P. Ho, and W. F. Degrado, Proteins: Struct., Funct., Genet. **1**, 16 (1986).
[5] W. F. DeGrado and J. D. Lear, J. Am. Chem. Soc. **107**, 7684 (1985).
[6] W. F. DeGrado, C. M. Summa, V. Pavone, F. Nastri, and A. Lombardi, Annu. Rev. Biochem. **68**, 779 (1999).
[7] T. Kortemme, M. Ramírez-Alvarado, and L. Serrano, Science **281**, 253 (1998).
[8] S. Marqusee, V. H. Robbins, and R. L. Baldwin, Proc. Natl. Acad. Sci. U.S.A. **86**, 5286 (1989).
[9] R. Aurora, T. P. Creamer, R. Srinivasan, and G. D. Rose, J. Biol. Chem. **272**, 1413 (1997).
[10] C. C. Lee, J. A. MacKay, J. M. J. Frechet, and F. C. Szoka, Nat. Biotechnol. **23**, 1517 (2005).
[11] G. I. Makhatadze and P. L. Privalov, Adv. Protein Chem. **47**, 307 (1995).
[12] J. P. Kemp and J. Z. Y. Chen, Biomacromolecules **2**, 389 (2001).
[13] J. Das, M. Yoshida, Z. M. Fresco, T.-L. Choi, J. M. J. Frechet, and A. K. Chakraborty, J. Phys. Chem. B **109**, 6535 (2005).
[14] J. P. Kemp and Z. Y. Chen, Phys. Rev. Lett. **81**, 3880 (1998).
[15] F. Wang and D. P. Landau, Phys. Rev. E **64**, 056101 (2001).
[16] A. G. Cunha-Netto, A. A. Caparica, S.-H. Tsai, R. Dickman, and D. P. Landau, Phys. Rev. E **78**, 055701 (2008).
[17] K. Ghosh and K. A. Dill, J. Am. Chem. Soc. **131**, 2306 (2009).
[18] S. Elli, F. Ganazzoli, E. G. Timoshenko, Y. A. Kuznetsov, and R. Connolly, J. Chem. Phys. **120**, 6257 (2004).
[19] S. J. Leach, G. Némethy, and H. A. Scheraga, Biopolymers **4**, 369 (1966).
[20] D. K. Christopoulos, A. F. Terzis, A. G. Vanakaras, and D. J. Photinos, J. Chem. Phys. **125**, 204907 (2006).
[21] Y. Kamikawa, T. Kato, H. Onouchi, D. Kashiwagi, K. Maeda, and E. Yashima, J. Polym. Sci., Part A-1 **42**, 4580 (2004).